AGU ADVANCING EARTH AND SPACE SCIENCES

Geophysical Research Letters

RESEARCH LETTER
10.1029/2024GL111403

Nonlinear Soil Moisture Loss Function Reveals Vegetation Responses to Water Availability

Ryoko Araki[1,2], Bryn E. Morgan[2,3], Hilary K. McMillan[1], and Kelly K. Caylor[2,4]

[1]Department of Geography, San Diego State University, San Diego, CA, USA, [2]Department of Geography, University of California, Santa Barbara, Santa Barbara, CA, USA, [3]Now at Department of Civil and Environmental Engineering, Massachusetts Institute of Technology, Cambridge, MA, USA, [4]Bren School of Environmental Science and Management, University of California, Santa Barbara, Santa Barbara, CA, USA

Key Points:

- A novel nonlinear soil moisture loss model outperforms a linear model in describing satellite-derived soil moisture across various landscape
- Globally, the nonlinearity parameter q greater than 1 dominates, indicating slower soil drying and conservative vegetation water-use
- The q values vary by vegetation type, with herbaceous vegetation showing a more aggressive water-use strategy

Supporting Information:

Supporting Information may be found in the online version of this article.

Correspondence to:

R. Araki,
raraki@ucsb.edu

Citation:

Araki, R., Morgan, B. E., McMillan, H. K., & Caylor, K. K. (2025). Nonlinear soil moisture loss function reveals vegetation responses to water availability. *Geophysical Research Letters*, *52*, e2024GL111403. https://doi.org/10.1029/2024GL111403

Received 29 JUL 2024
Accepted 21 MAY 2025

Abstract Soil moisture drydown patterns encode signatures of vegetation water-use. Previous characterizations of the drydown patterns assume a static linear relationship between water-limited transpiration and available moisture. However, ecohydrological studies show that vegetation exhibits a spectrum of responses to water availability, suggesting that soil moisture loss functions may be nonlinear. To represent these dynamics, we introduce a nonlinearity parameter to the loss function. Our analysis shows that the nonlinear loss model improves the characterization of the satellite-observed soil moisture drydowns. Globally, functional responses of drydowns are dominated by convex nonlinearity, showing less ecosystem water loss in dry soils than the linear loss function predicts. We find distinct degrees of nonlinearity among different vegetation types; areas with non-woody vegetation more frequently exhibit a concave nonlinearity, the signature of aggressive water-use strategies. We propose the nonlinear loss function as a continuous and dynamic framework to represent vegetation water-use under changing water availability.

Plain Language Summary Patterns of soil moisture decline after rainfall contain signatures of how much vegetation transpires. In this study, we modified an existing theory relating soil moisture declines and evapotranspiration by introducing a nonlinearity parameter to the relationship. We applied this novel method to global satellite soil moisture data, confirmed the performance, and showed that the results are consistent with the previous understandings of interactions between soil moisture and the surrounding environments. In particular, our model successfully captures how vegetation uses water more aggressively or conservatively under varying water availability at landscape scale. This novel method allows us to characterize vegetation water-use and their vulnerability to drought conditions at the global scale.

1. Introduction

Vegetation water-use plays a critical role in global terrestrial water (Jung et al., 2010), energy (Lei et al., 2018), and carbon cycles (Green et al., 2019). Plants passively uptake water through the gradient of water potential from soil to roots to leaves to atmosphere; consequently, soil water availability is a key limiting factor of vegetation water-use. Water limitations on vegetation water-use have typically been characterized by a static threshold, θ_*, at which plants begin to reduce transpiration (Bassiouni et al., 2020a, 2020b; Dong et al., 2022; Feldman et al., 2019; Fu et al., 2022, 2024); however, this down-regulation of transpiration is more continuous and continues below the threshold θ_* (Hochberg et al., 2018; Wilkening et al., 2024). Understanding these dynamic plant responses is vital for the prediction of ecosystem behaviors during droughts (Berg & Sheffield, 2018) and for agricultural applications (Stocker et al., 2019), but characterizing them at landscape scales has been challenging (Konings & Gentine, 2017; Y. Li et al., 2017).

Vegetation water-use signals are encoded in the drying rate of soil moisture (Abolafia-Rosenzweig et al., 2020; Small et al., 2018), which can be quantified using the soil moisture loss function $L(\theta, t)$. $L(\theta, t)$ is a function that describes the rate of water loss from the soil volume at the landscape scale, driven by a combination of ecohydrological processes, including gravity drainage, runoff, and evapotranspiration (see Section 2.1 for the detailed definition). The soil moisture loss function $L(\theta, t)$ relates drydown rate for a given moisture content, and is dominated by evapotranspiration processes from a few days after rainfall (McColl et al., 2017). As soil moisture drops below the field capacity θ_{fc}, soil moisture loss due to evapotranspiration (ET) dominates at its maximum rate ET_{max} until a critical value of soil moisture, θ_*, is reached. Below θ_*, plants begin to close stomata and regulate transpiration, and therefore soil moisture loss due to ET is limited by water availability as:

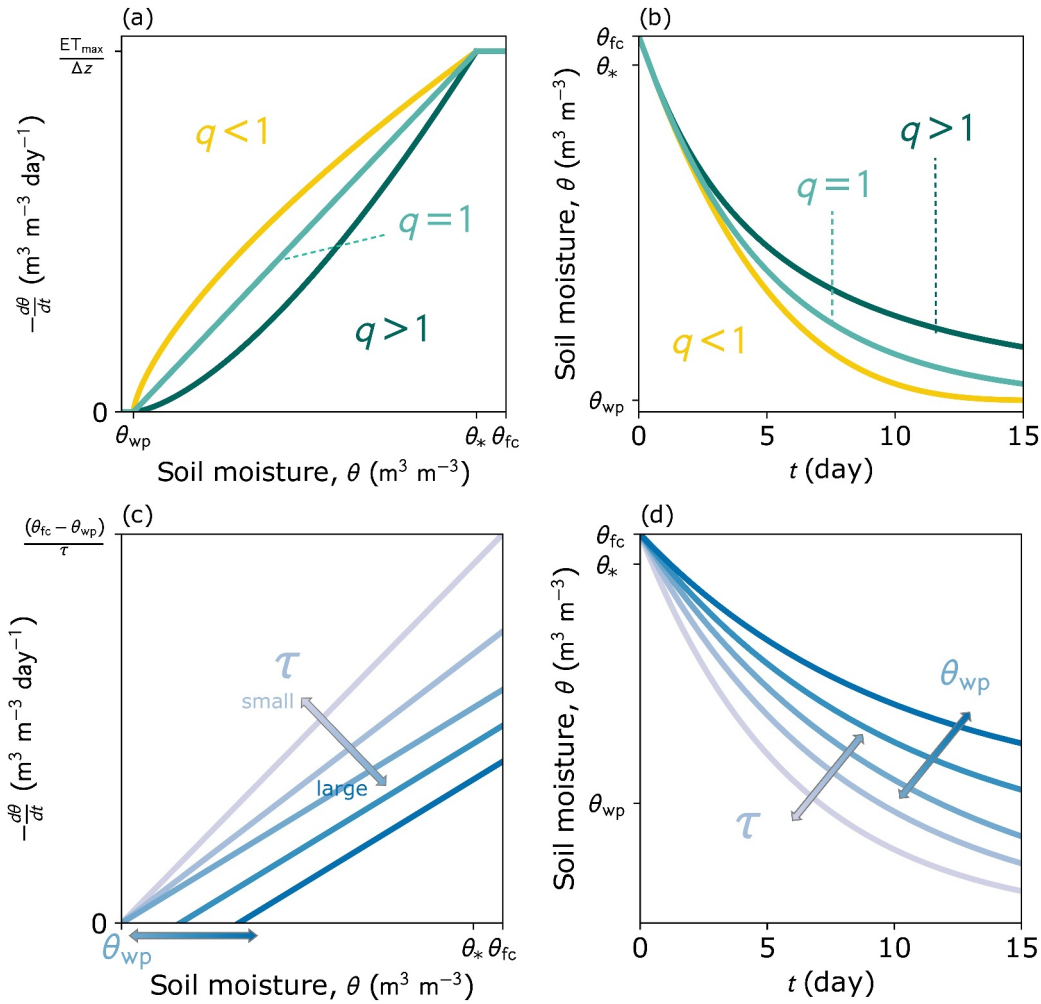

Figure 1. Conceptual figure of linear ($q = 1$) and nonlinear ($q \neq 1$) loss models (a) in the soil moisture loss functions space, normalized by soil thickness Δz as $\frac{L(\theta,t)}{\Delta z} = -\frac{d\theta}{dt}$, and (b) in the time domain. Conceptual figure of the τ-based characterization of the drydown (c) in the normalized loss function space and (d) in the time domain.

$$L(\theta, t) = -\Delta z \frac{d\theta}{dt} = \mathrm{ET}_{\max} \left(\frac{\theta(t) - \theta_{\mathrm{wp}}}{\theta_* - \theta_{\mathrm{wp}}} \right)^q, \tag{1}$$

where the parameter q (−) represents the degree of nonlinearity of the soil moisture loss function (Figures 1a and 1b).

Most hydrologic studies assume $q = 1$ (Figure 1a, $q = 1$), meaning that the soil moisture loss function dictates the linear relationship between available soil moisture and ET. This linear assumption was initially made to represent soil moisture dynamics in arid climates, where ET is limited primarily by water availability rather than energy supply (Laio et al., 2001; Rodriguez-Iturbe et al., 1999). The popularity of linear assumption has grown due to its simplicity and ease of integration. The analytical solution of Equation 1 yields a straightforward exponential function of time (Shellito et al., 2016) (Figure 1b, $q = 1$), making it suitable for probabilistic (Laio, 2002; Rodriguez-Iturbe et al., 1999) and spatio-temporal (Entekhabi & Rodriguez-Iturbe, 1994; Teuling & Troch, 2005) analysis of soil moisture dynamics. The decay timescale τ in this exponential function is useful for analyzing soil moisture dissipation and its coupling with land-atmosphere processes as well (Koster & Suarez, 2001; McColl et al., 2019; Rahmati et al., 2024). This linear soil moisture loss function has been applied to remote-sensing soil moisture products and advanced our understanding of critical aspects of soil-vegetation-atmosphere dynamics. Examples include defining dynamic regimes of soil moisture (Akbar et al., 2018;

Sehgal et al., 2021), investigating the hydroclimatic and physiographic drivers of the dynamics (Bassiouni et al., 2020a, 2020b; Shellito et al., 2018), and comparing the dynamics captured by satellite and in-situ observation (Rondinelli et al., 2015; Tso et al., 2023).

However, a linear assumption ($q = 1$) may not be the most appropriate representation of vegetation responses to soil moisture availability, especially when applied globally. For example, the soil moisture loss function could show a nonlinear response ($q \neq 1$) when vegetation either conserves or aggressively consumes water in response to changing soil moisture conditions (McDowell et al., 2008). Experimental (Meinzer et al., 2016) and remote-sensing studies (Bassiouni et al., 2020a, 2020b; Feldman et al., 2018) suggest that vegetation can exhibit widely varying water-use strategies in response to water deficit. Indeed, ecohydrological studies have represented nonlinear vegetation water responses to water availability, including vegetation water stress as a power function of available soil moisture (Porporato et al., 2003) and transpiration down-regulation as a sigmoid function of soil moisture (Bassiouni et al., 2023). These studies suggest that approaches that explicitly account for nonlinear vegetation behaviors provide a more robust representation of ET and enable insights into vegetation responses to water stress from soil moisture data at landscape scale.

Here, we propose a nonlinear soil moisture loss function, allowing $q \neq 1$ in Equation 1, grounded in ecohydrology that offers a more dynamic representation of ET as a function of soil moisture content (Figure 1a). When $q < 1$, the soil moisture loss function is concave, reflecting lower sensitivity of ecosystem water loss to initial declines in soil moisture, and a more aggressive vegetation water-use at low available soil moisture. Conversely, $q > 1$ describes a convex soil moisture loss function, which exhibits greater sensitivity of ecosystem water loss to initial soil moisture declines, and more conservative vegetation water-use at low available soil moisture. These variations in the loss function shape result in either faster or slower soil moisture drydowns relative to the linear loss model (Figure 1b), allowing us to detect changes in q values from the timeseries of soil moisture drydowns.

The primary objective of this study is to investigate the applicability of the nonlinear soil moisture loss function to characterize satellite soil moisture drydowns. First, we compare the linear and nonlinear approaches to describe drying patterns of satellite soil moisture data retrieved from the Soil Moisture Active Passive (SMAP) radiometer. Second, we investigate whether the strength of nonlinearity in the soil moisture loss function, q, reflects expected patterns of interaction with climate, soil texture, and vegetation types. Specifically, we examine whether the expected responses of vegetation to water availability can be captured by the nonlinearity parameter q. The first part of the analysis also includes an examination of the popular exponential decay drydown model. The linear drydown model is often parameterized using the exponential decay timescale τ (Figures 1c and 1d), which is equivalent to $\frac{\Delta z(\theta_* - \theta_{wp})}{ET_{max}}$ based on Equation 1; this τ-based linear model was incorporated in model performance comparison.

2. Methods

For simplicity, the soil moisture drydown models that assume linear and nonlinear loss functions are hereafter referred to as "linear loss model" and "nonlinear loss model," respectively. The linear loss model parameterized with τ is referred to as "τ-based linear loss model." All analyses are performed at the scale of satellite soil moisture data from Soil Moisture Active-Passive (SMAP) radiometer based on the Equal-Area Scalable Earth (EASE) Grid, referred to as the "SMAP grid."

2.1. Soil Moisture Loss Function

Assuming a planar, homogeneous soil, soil moisture dynamics are described by a vertically integrated water balance equation (Laio et al., 2001; Rodriguez-Iturbe et al., 1999) according to,

$$\Delta z \frac{d\theta(t)}{dt} = P(t) - L(\theta, t), \tag{2}$$

where θ is volumetric soil water content [$m^3\ m^{-3}$] at time t [s], Δz is the thickness of the soil [m], $P(t)$ is the precipitation rate [$m\ s^{-1}$], $L(\theta, t)$ is the rate of water loss from the soil volume [$m\ s^{-1}$], which is called a soil moisture loss function (Laio et al., 2001; Rodriguez-Iturbe et al., 1999).

The soil moisture loss function summarizes processes that cause water loss from the soil volume and is typically divided into three stages: Drainage, Stage I ET, and Stage II ET losses.

$$L(\theta,t) = \begin{cases} D(\theta,t) + Q(\theta,t) + \mathrm{ET}_{\max}, & \theta_{\mathrm{fc}} \le \theta(t) \\ \mathrm{ET}_{\max}, & \theta_{*} \le \theta(t) < \theta_{\mathrm{fc}} \\ \mathrm{ET}(\theta,t), & \theta_{\mathrm{wp}} \le \theta(t) < \theta_{*} \end{cases} \tag{3}$$

The Drainage stage occurs during the wettest conditions, when the soil moisture, $\theta(t)$, is greater than the field capacity, θ_{fc} (i.e., $\theta_{\mathrm{fc}} \le \theta(t)$). In this case, ET at its maximum rate $\mathrm{ET}_{\max}$, gravity drainage from the bottom boundary of the soil layer $D(\theta,t)$, and surface runoff $Q(\theta,t)$ all contribute to the soil moisture loss. In Stage I ET, as soil moisture drops below the field capacity θ_{fc}, drainage and surface runoff become negligible. However, ET continues at $\mathrm{ET}_{\max}$ until a critical value of soil moisture, θ_{*}, is reached (i.e., $\theta_{*} \le \theta(t) < \theta_{\mathrm{fc}}$). The condition $\theta(t) = \theta_{*}$ marks the end of Stage I and the beginning of Stage II ET, which represents the water-limited stage, where ET is limited by soil water availability, $\mathrm{ET}(\theta,t)$. Stage II ET continues until the soil moisture reaches the wilting point, θ_{wp} (i.e., $\theta_{\mathrm{wp}} \le \theta(t) < \theta_{*}$). This dynamics of water-limitation on ET is expressed as the function of soil water availability, previously introduced as Equation 1.

Since the Drainage stage and Stage I ET occur rapidly, we can assume that soils are in Stage II ET most of the time for satellite-observed soil moisture data with 2–3 days temporal resolution (McColl et al., 2017). Additionally, evaporation may still occur below θ_{wp} down to the hygroscopic point θ_{h}; however, since the true values of θ_{wp} and θ_{h} are close, the effect of this difference is assumed to be minimal for the satellite data analysis.

2.2. Drydown Models for Stage II ET Losses

An analytical solution of the soil moisture loss function in Equation 1 gives the drydown models of soil moisture over time (See Text S1 in Supporting Information S1 for derivation). When $q = 1$, the analytical solution is a simple exponential function of time given as:

$$\theta(t) = (\theta_0 - \theta_{\mathrm{wp}})\, e^{-\frac{\mathrm{ET}_{\max}}{\Delta z(\theta_{*}-\theta_{\mathrm{wp}})}t} + \theta_{\mathrm{wp}}, \tag{4}$$

and we call this linear loss model. Here, $\theta(t)$ is a volumetric soil moisture content observed t days after the start of the drydown, and θ_0 [$\mathrm{m}^3\ \mathrm{m}^{-3}$] is the initial soil moisture value.

When $q \neq 1$, the analytical solution of Equation 1 takes a different form:

$$\theta(t) = \left[-\frac{\mathrm{ET}_{\max}}{\Delta z} \frac{1-q}{(\theta_{*}-\theta_{\mathrm{wp}})^{q}}\, t + (\theta_0 - \theta_{\mathrm{wp}})^{1-q} \right]^{\frac{1}{1-q}} + \theta_{\mathrm{wp}}, \tag{5}$$

and we call this a nonlinear loss model. The parameters $\mathrm{ET}_{\max}$, θ_{*}, and θ_{wp} determine the slope $(\mathrm{ET}_{\max}/(\theta_{*} - \theta_{\mathrm{wp}}))$, and the parameter q controls the degree of nonlinearity of the θ-$-\frac{d\theta}{dt}$ relationship as illustrated in Figure 1a. This function is undefined at a value of $q = 1$, as this leads to the exponent being ∞.

Conceptually, the nonlinearity parameter q quantifies emergent patterns of plant responses to water deficits at landscape scale, reflecting their aniso- and iso-hydric strategies (Tardieu & Davies, 1993; Tardieu & Simonneau, 1998); when soil water potential drops, plants taking anisohydric strategies keep their stomata open to maintain transpiration and prioritize productivity, while those taking isohydric strategies close stomata to reduce transpiration and prevent xylem cavitation.

The drydown model in Equation 4 is commonly denoted as (McColl et al., 2017; Shellito et al., 2016; Small et al., 2018):

$$\theta(t) = \Delta\theta e^{-\frac{t}{\tau}} + \theta_{\mathrm{wp}}, \tag{6}$$

and we call this τ-based linear loss model. Here, $\Delta\theta$ is the initial soil moisture content above the wilting point [m^3 m^{-3}], and τ [s^{-1}] is the decay rate of soil moisture. This is the same equation of the linear loss model (Equation 4) but with different parametrization, where $\Delta\theta = \theta_0 - \theta_{wp}$ and $\tau = \frac{\Delta z(\theta_* - \theta_{wp})}{ET_{max}}$. In other words, three parameters θ_*, θ_{wp}, and ET_{max}, were aggregated to a single parameter, τ, in this model.

The τ-based model offers similar or greater flexibility compared to the nonlinear model, while differing in its functional form. The nonlinear model allows changes in both the slope and concavity of the function (Figures 1a and 1b); whereas the τ-based model allows changes in slope and the convergence point of the drydown curve, θ_{wp}, for each event (Figures 1c and 1d). The τ-based linear model also imposes fewer constraints on ET_{max} and θ_*.

2.3. Identification of Drydown Events and Model Fitting

Drydown events are identified as periods of consistent moisture decrease. An event starts when the prior positive increment exceeds the target unbiased root-mean-square (ubRMSE) for SMAP data (0.04 m^3 m^{-3}), and ends with a positive increment over 5% of the historical soil moisture range at the SMAP grid (McColl et al., 2017) or when precipitation exceeds 2 mm (Shellito et al., 2016; Small et al., 2018) (See Text S2 in Supporting Information S1).

For each drydown event, models (Equations 4–6) are fitted using nonlinear least squares (Virtanen et al., 2020). Large soil moisture values greater than field capacity θ_{fc} previously estimated from SMAP 36 km data (Bassiouni, 2020) are masked. The drydown trajectory is fitted to a piecewise function, consisting of Stage I ET $\left(\theta(t) = \theta_0 - \frac{ET_{max}}{\Delta z}t\right)$ and Stage II ET losses (Equations 4 and 5). For the τ-based linear loss model (Equation 6), however, the threshold between Stages I and II ET losses (θ_*) is implicit in τ; therefore, the model was fitted to the entire drydown trajectory.

The estimated parameters are ET_{max}, θ_*, and θ_0 for the linear loss model, and additionally q for the nonlinear loss model. For the τ-based linear loss model, we estimated τ, θ_{wp}, and $\Delta\theta$. Hereafter, the estimated parameters are indicated with hat (e.g., $\hat{q}$ indicates estimated q values). Parameters are constrained to physically plausible values (See Text S3 in Supporting Information S1). Drydown events were filtered for goodness-of-fit $\left(R^2 > 0.8\right)$ and excluded if soil moisture ranges cover <20% of the historical range, or exhibit spuriously slow or rapid drydowns (See Text S4 in Supporting Information S1).

3. Data

We conduct all analyses at a spatial resolution of 36-km SMAP grid with the 7-year period from 1 April 2015 to 31 March 2022. We analyze surface soil moisture drydown patterns using data from the National Aeronautics and Space Administration's (NASA) Soil Moisture Active-Passive (SMAP) mission (O'Neill, Chan, et al., 2021). SMAP L3 product provides daily soil moisture for the top 5 cm layer at 36 km spatial resolution. Data flagged due to precipitation, snow, open water, urban development, frozen ground, steep hills, and high vegetation density (>5 kg m^{-2}) are excluded from the analysis. The average daily precipitation depth estimate is calculated from the 3-hourly 9-km SMAP L4 product (Reichle et al., 2022).

We investigate the relationships between the estimated parameters ($\hat{q}$, $\widehat{\theta_*}$, $\widehat{ET_{max}}$) of the loss model with climate, soil texture, and vegetation types. Climates are represented using an aridity index, calculated as the mean annual precipitation divided by the mean annual PET (Greve et al., 2019) averaged for the study period. Daily PET data at 0.1-degree spatial resolution are obtained from the dPET data set (M. B. Singer et al., 2021; M. Singer et al., 2020). Sand fraction, representing soil characteristics, and International Geosphere-Biosphere Programme (IGBP) landcover data, representing vegetation types, are obtained from the SMAP ancillary static data set (Peng et al., 2019).

Previous studies point out that a global categorical land-cover data set sourced from remote-sensing data, such as IGBP, is a poor predictor of vegetation-water dynamics (Konings & Gentine, 2017; Y. Li et al., 2017). In this study, we additionally utilize a CONUS-scale rangeland data set, Yearly 30-m Rangeland Analysis Platform Vegetation Cover Data Version 3, which provides detailed information on functional vegetation type and preserves its spatial heterogeneity sourced from both remote-sensing and field data (Allred et al., 2021). We computed total vegetation cover as the sum of four types: annual forbs and grasses, perennial forbs and grasses,

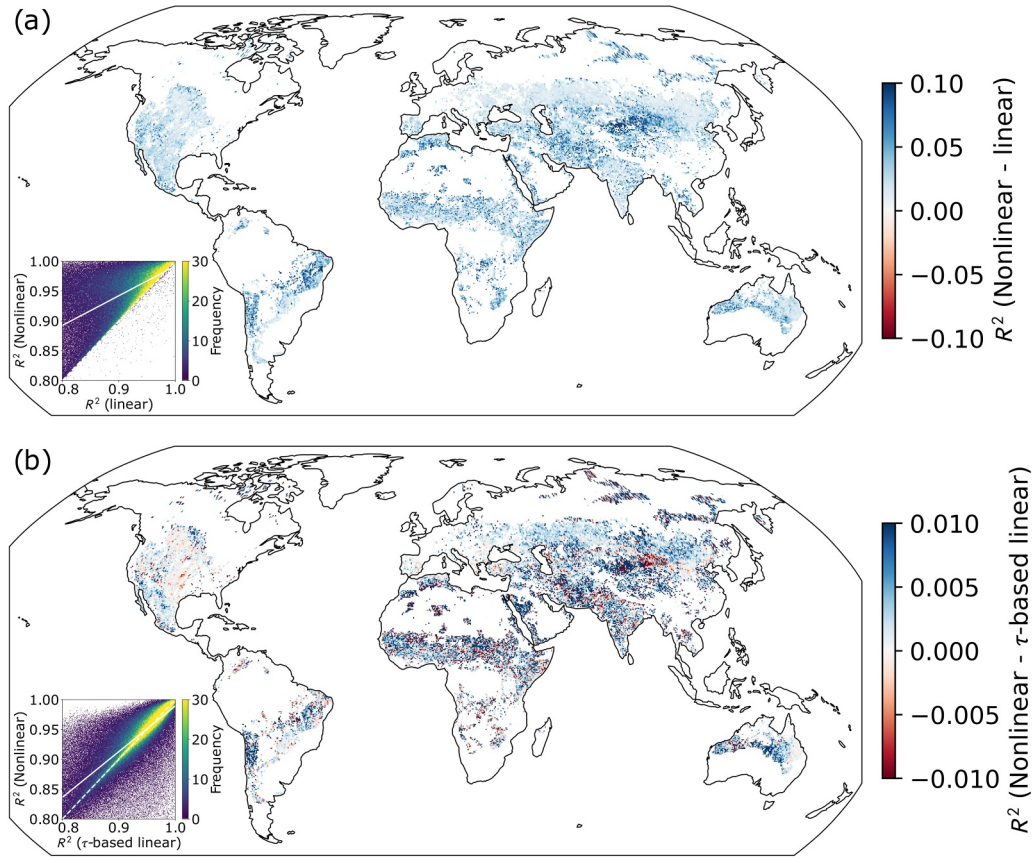

Figure 2. Comparison of model fit. The maps display the median R^2 differences per SMAP grid between (a) the nonlinear and linear loss models, and (b) the nonlinear and τ-based linear loss models. Areas with higher values (blue) indicate that the nonlinear loss model yields smaller residuals, reflecting improved model fitting. White areas indicate either the absence of data or a lack of a qualified drydown event. The subplots within the maps display scatter plots of R^2, with dashed lines representing the 1:1 line and solid lines representing the linear trendline.

shrubs, and trees; thereby excluding barren, litter, and non-rangeland covers. The wood fraction of the vegetated area is then calculated as the percent of woody coverage (shrubs and trees) relative to the total vegetation cover.

4. Results and Discussion

4.1. Performance of the Nonlinear Drydown Model

We evaluated the fit of the nonlinear loss model compared to the two linear models. Figure 2 illustrates the differences in the model's goodness-of-fit, R^2, to SMAP soil moisture drydown events. As expected, with one additional degree of freedom, the nonlinear loss model achieves better R^2 values than the linear model by definition (Figure 2a); the shading on the map indicates the magnitude of the improvement, which reflects how much the loss function deviates from linearity. When compared to the τ-based linear model, the nonlinear loss model (Figure 2b) showed better R^2 in 59.8% of qualified events ($n = 499{,}732$) and 71.8% of studied SMAP grids ($n = 31{,}886$). We further assessed the model performance using the Akaike Information Criterion, *AIC* (Akaike, 1974), which accounts for the trade-off between goodness-of-fit and model complexity (Text S5 in Supporting Information S1). Compared to the linear model (Figure S2a in Supporting Information S1), the nonlinear model outperformed in 43.3% of qualified drydown events ($n = 367{,}789$), and 35.3% of studied SMAP grids ($n = 30{,}370$) in *AIC*. The performance of the nonlinear model, both in terms of R^2 and *AIC*, declines in deserts (e.g., Sahara, Gobi) and agricultural regions (e.g., central India, U.S. Great Plains), potentially due to SMAP data uncertainty or other processes (Text S6 in Supporting Information S1).

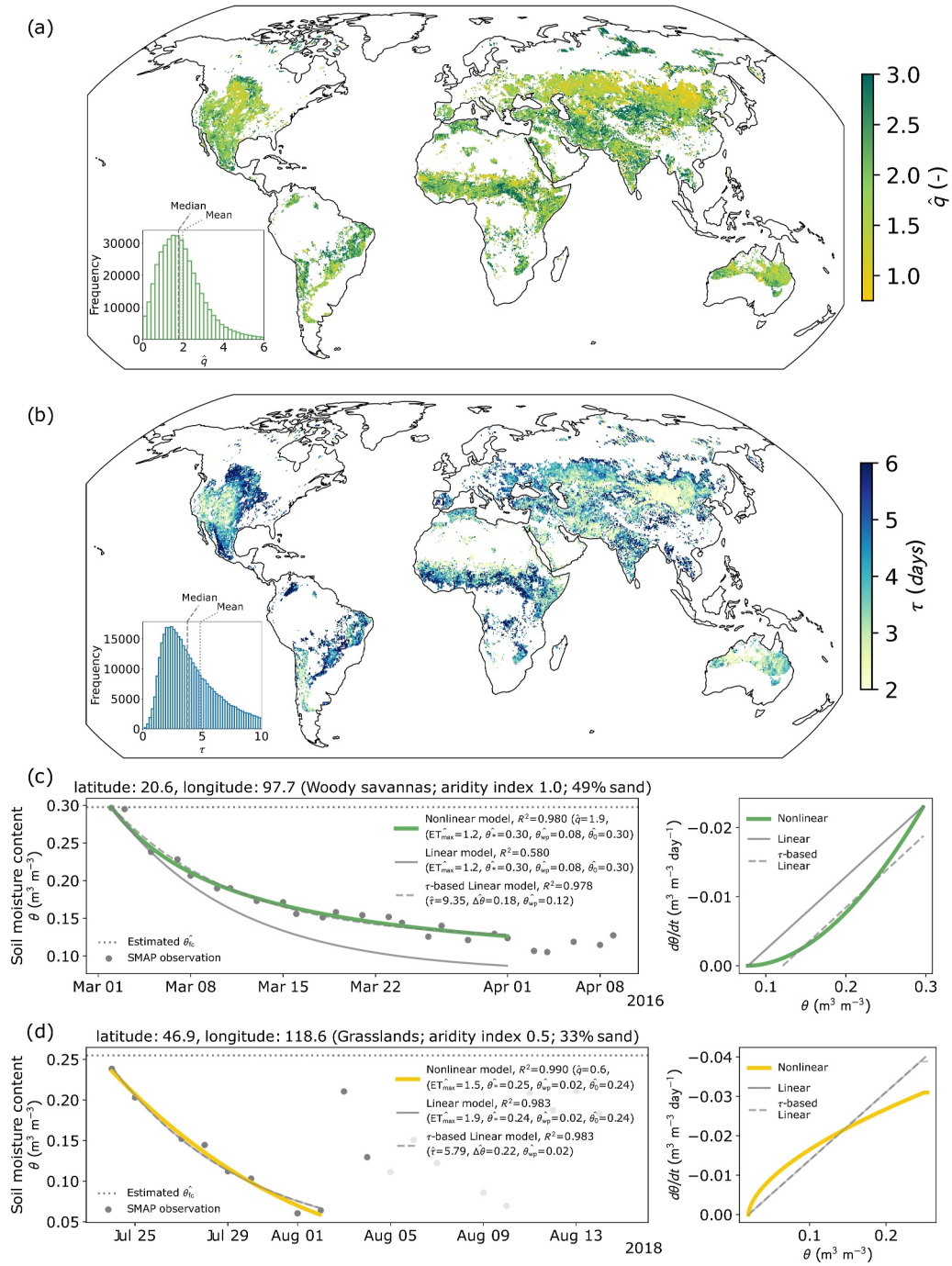

Figure 3. Spatial patterns of the nonlinear parameter $\hat{q}$ and its role in characterizing drydowns. (a) The map displays the median $\hat{q}$ values per SMAP grid with the histogram. Areas with higher values ($\hat{q} > 1$, darker green) indicate a stronger convex soil moisture loss function and conservative vegetation water-use, while lower values ($\hat{q} < 1$, yellow) indicate a stronger concave loss function and aggressive water-use. White areas indicate either the absence of data or a lack of a qualified drydown event. See Figure S8 in Supporting Information S1 for the map of other estimated parameters. (b) The map displays the median $\hat{\tau}$ values per SMAP grid with the histogram from the τ-linear loss model. (c, d) Model fits to the observed soil moisture drydown events in the time domain (left) and in the loss-function space (right) for the cases of (b) $\hat{q} > 1$ and (c) $\hat{q} < 1$.

There is an improvement in *AIC* and R^2 in areas with a range of $\hat{q}$ values (Figure 3a), suggesting that the nonlinear loss model effectively captures both convex ($\hat{q} < 1$) and concave ($\hat{q} > 1$) curvature in soil moisture loss patterns. The median and average global $\hat{q}$ values are 1.76 and 1.97, respectively, and the distribution is positively skewed.

This global prevalence of convex nonlinear loss function ($\hat{q} > 1$) indicates that the soil moisture drydown decelerates more than previously estimated by the linear loss model. In other words, the linear loss model tends to overestimate the ET rate as the soil dries, compared to the nonlinear model (Figure 3c). Conversely, in the regions with $\hat{q} < 1$, the linear models tend to underestimate the ET as the soil dries (Figure 3d).

Several factors in satellite remote-sensing data may have impacted the performance of the nonlinear model and signals of $\hat{q}$. The standard t-test indicated that the $\hat{q}$ value significantly ($p < 0.05$) deviates from 1 only less than 10% of the events (Text S7 in Supporting Information S1), suggesting that the $\hat{q}$ values are either obscured by spatio-temporal scale of satellite measurement, or only temporarily deviate from 1. The $\hat{q}$ values represent the averaged signals of drydowns from heterogeneous landscapes within the SMAP radar's footprint. Additionally, model fitting is also influenced by 2–3 days retrieval intervals, further compounded by data uncertainty. To overcome these, future studies can extend the current method to other soil moisture timeseries, such as high-frequency in-situ soil moisture observations. Furthermore, because q can be quantified per a drydown event, its variation over time can be analyzed as well.

Nonetheless, the characteristics of the nonlinear loss model, compared to the linear models, are in how they map changes in drydowns patterns within the loss function space (Figures 3c and 3d). The linear loss model, which relies on the $\widehat{\theta_*}$ value as a threshold of stomatal closure, fails to capture the curvature in the drydowns. The τ-based linear model reflects the changes in drydown patterns as shifts in the θ-axis ($\widehat{\theta_{wp}}$) and changes in slope ($1/\hat{\tau}$) of the loss function, whereas the nonlinear model expresses them as changes in curvature ($\hat{q}$) and slope ($\widehat{ET_{max}}/(\widehat{\theta_*} - \widehat{\theta_{wp}})$). Due to these characteristics, $\widehat{\theta_{wp}}$ in the τ-based model could be biased toward the observed minimum $\theta(t)$ values during a drydown event. In contrast, the nonlinear model can utilize changes in curvature $\hat{q}$ as an indicator of functional response, without unrealistically altering $\widehat{\theta_{wp}}$ for each event. As a result, the $\hat{q}$ and $\hat{\tau}$ values exhibit distinct spatial patterns as well (Figures 3a and 3b). The superior performance of the nonlinear model in some regions, even under stricter parameter bounds, suggests that it captures information beyond the capability of the linear loss model. The next section explores the implications of the estimated parameters from the nonlinear loss model.

4.2. Relationships Between Estimated Ecohydrological Parameters With Environmental Variables

Ecosystem loss estimated from the satellite soil moisture is primarily driven by evapotranspiration, rather than gravity drainage or runoff (McColl et al., 2017); the correlations between the parameters estimated from the nonlinear loss model and environmental variables (climate, soil texture, and vegetation types) are consistent with this process understanding (Figures 4a and 4b; see also Figure S9 in Supporting Information S1). The observed decreases in $\widehat{\theta_*}$ with decreasing aridity index (Spearman's rank correlation coefficient $\rho = 0.73$) aligns with the fact that vegetation in more arid climates begins stomatal closure at lower soil moisture levels. Similarly, decreases in $\widehat{\theta_*}$ with increasing sand fraction ($\rho = -0.36$) may be reflecting decreases in field capacity θ_{fc} below which θ_* occurs. Increases in $\widehat{ET_{max}}$ with decreasing aridity index ($\rho = -0.32$) are expected, where PET is higher in drier climates.

In contrast, the nonlinear parameter $\hat{q}$ exhibits a very weak correlation with the aridity index ($\rho = 0.04$) and sand fraction ($\rho = 0.01$). Rather, $\hat{q}$ values significantly differ across vegetation types ($p < 0.01$, Figure S10 in Supporting Information S1), and are higher in woody vegetation classes (Figure 4c, Grassland < Croplands < Open shrublands < Woody savannah and savannah). The CONUS-scale analysis using detailed vegetation data reveals that, within each climate class, the proportion of drydown events exhibiting $\hat{q} < 1$ increases with a decreasing wood fraction of vegetated area (Figure 4d). This trend in $\hat{q}$ values remains robust even after accounting for the impacts of event duration and non-vegetated land-cover (see Text S8 in Supporting Information S1).

The CONUS-scale analysis (Figure 4d) focuses on SMAP grids with more than 80% vegetation cover, therefore, the estimated ecosystem loss derived from the model is likely dominated by transpiration (Good et al., 2015; Jasechko et al., 2013). The prevalence of $\hat{q} < 1$ events in areas dominated by non-woody vegetation suggests that the nonlinear loss model effectively captures dynamics where vegetation maintains high transpiration rates under low soil moisture conditions. These findings align with previous global-scale studies, which show that non-woody, herbaceous vegetation types are generally more anisohydric and aggressive water-users, continuing to transpire under drier conditions (Bassiouni et al., 2020a, 2020b; Konings & Gentine, 2017; Y. Li et al., 2017). The

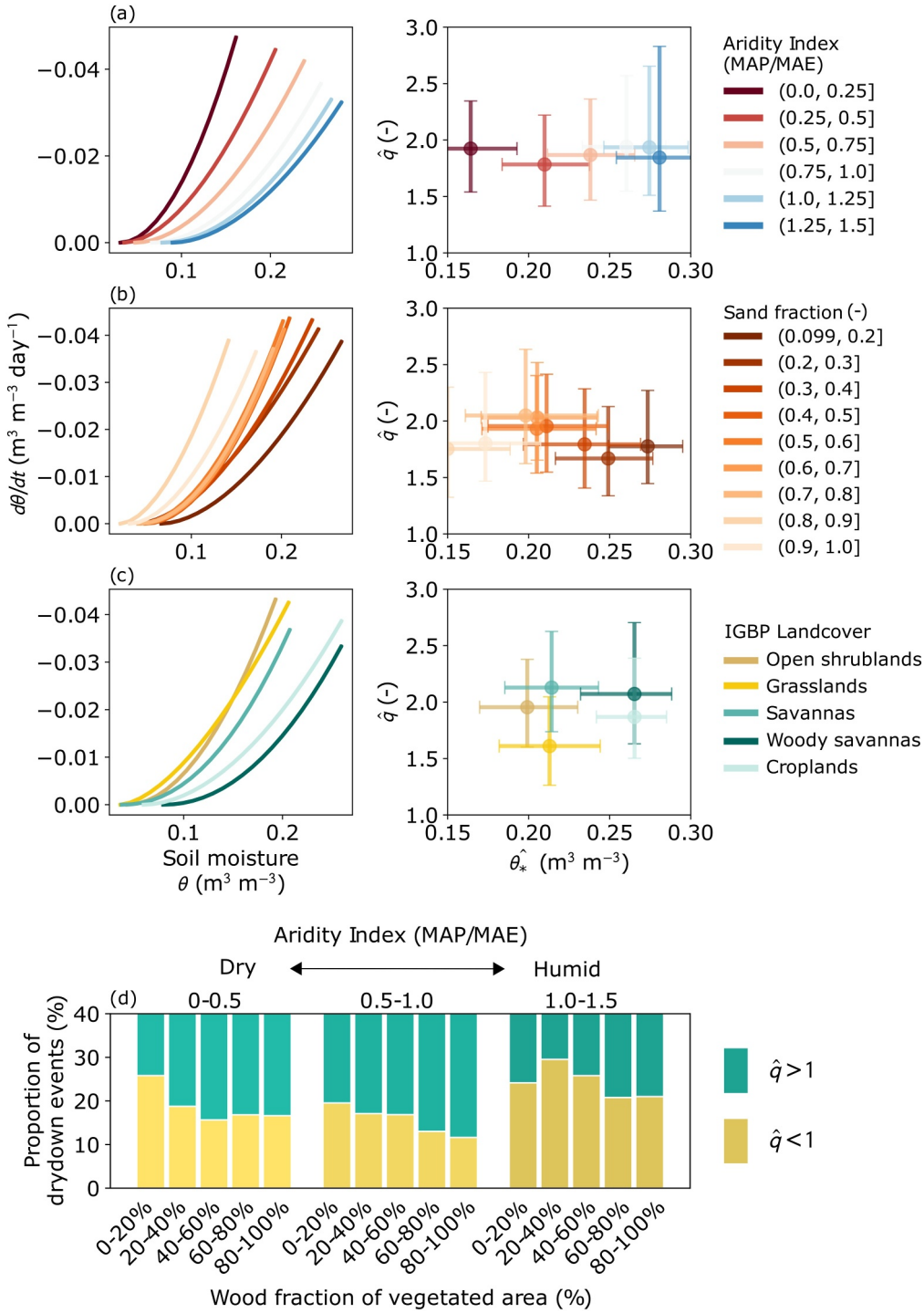

Figure 4. Nonlinear loss function characteristics according to climate (a), soil (b), and vegetation types (c, d). The left panels from (a–c) show the reconstructed Stage II ET nonlinear loss functions. Panel (d) shows the proportion of drydown events that exhibit $\hat{q} < 1$ or $\hat{q} > 1$ by the aridity index (mean annual precipitation, MAP, over mean annual evaporation, MAE) and the wood fraction of vegetated area.

$\hat{q} < 1$ pattern we identified contrasts with soil water loss dominated by evaporation, which follows an exponential function (Krell et al., 2021) resembling $\hat{q} > 1$ nonlinearity. In light of this, $\hat{q} < 1$ may serve as a signature of the differential responses of non-woody and woody vegetation to available water. Here, our analysis focused on regions where SMAP data are known to be reliable (Colliander et al., 2017, 2022; O'Neill, Bindlish, et al., 2021),

which excludes forested or steep hillslope regions. Including these ecosystems may show even stronger patterns of $\hat{q}$ by wood fractions that we see in Figure 4d.

4.3. Functional Importance of Nonlinear Vegetation Response

The utility of the nonlinear framework lies not in its fitting performance but in its ability to describe underlying ecosystem processes. Introducing nonlinearity adds complexity to the existing linear loss model, which may hinder the model's performance in predictive mode. Despite these limitations, however, the nonlinear model learns and captures the degree of nonlinearity, q, from the observed soil moisture data, describing whether vegetation is saving water (convex nonlinearity) or consuming it (concave nonlinearity). Although these behaviors are well-studied at an individual plant scale in controlled experiments (Tardieu & Davies, 1993; Tardieu & Simonneau, 1998), those at landscape scales have been challenging to characterize. The nonlinear loss model would allow us to investigate the vegetation water-use regulation on this broader ecosystem scale.

While this study interprets surface soil moisture as water sources for vegetation, we acknowledge that vegetation may access water from deeper soil layers (Fan et al., 2017), which may influence $\hat{q}$ (Teuling et al., 2006). However, the spatial variability of $\hat{q}$ that we found (Figure 3a) are not consistent with the spatial patterns of groundwater depth (Fan et al., 2013), or the regions where deeper soil moisture strongly controls vegetation productivity (W. Li et al., 2021). Furthermore, the majority of root biomass are concentrated within the top soil layers across ecosystems (Jackson et al., 1996). Our findings align with recent studies showing that surface soil moisture observation from satellites can effectively capture vegetation-water dynamics (Feldman et al., 2023; Feldman, Konings, et al., 2024; Feldman, Koster, et al., 2024).

Regulation of vegetation water-use has been often characterized using a static threshold-based approach, where the incipient stomatal closure point, θ_*, serves as a threshold indicator of water stress (Bassiouni et al., 2020a, 2020b; Fu et al., 2024). However, plants could respond gradually or abruptly to water availability below this threshold until the complete stomatal closure point, θ_{wp}. The q parameter in our nonlinear loss function are designed to capture these processes, providing a continuous, dynamic, and ecohydrologic characterization of vegetation water-use regulation. This q will be a valuable tool to identify vegetation water-use across climate zones and plant functional types, and predict which ecosystems are more sensitive to future climate change and soil moisture droughts.

5. Conclusions

We modified the soil moisture loss function to capture changing ecosystem water-use in response to water availability, by introducing a nonlinearity parameter q. Our analysis using SMAP satellite soil moisture data demonstrates that our nonlinear loss function improves the characterization of the majority of drydown events across regions. Globally, soil moisture declines are dominated by a convex nonlinear loss function ($\hat{q} > 1$), representing a higher sensitivity of evapotranspiration (ET) as the soil dries out; this implies that ET at an event scale may be overestimated if we continue to use the linear assumption. Additionally, the nonlinear parameter shows relationships with vegetation types that are consistent with their known functional responses to water limitation. In particular, soil moisture dynamics in landscapes dominated by non-woody vegetation are more often concave in their loss function ($\hat{q} < 1$), a signature of more aggressive vegetation water-use; conversely, woody landscapes yield the signatures of more conservative vegetation water-use ($\hat{q} > 1$). These findings illustrate how this nonlinear framework offers insights into dynamic and nuanced functional responses of vegetation to changing water availability.

Data Availability Statement

All codes used in this study are available via (Araki et al., 2025). All data used in this study are openly available from the following sources: SMAP soil moisture data (SPL3SMP, v8; O'Neill, Bindlish, et al., 2021; O'Neill, Chan, et al., 2021); SMAP precipitation data (SPL4SMGP, v7; Reichle et al., 2022); the SMAP ancillary static data set, containing sand fraction and IGBP land cover data (SMAP_L1_L3_ANC_STATIC; Peng et al., 2019); dPET data (Singer et al., 2020, 2021); Rangeland Analysis Platform Vegetation Cover Data (Allred et al., 2021).

Acknowledgments
Morgan and Caylor were supported by a grant from the Zegar Family Foundation (SB220237). Computations were performed on the University of California, Santa Barbara General Research IT (GRIT) computing systems. We thank Andrew Feldman and an anonymous reviewer for their valuable feedback. We express our gratitude to Naomi Christina Tague and Trent Biggs for their helpful comments and suggestions.

References

Abolafia-Rosenzweig, R., Badger, A. M., Small, E. E., & Livneh, B. (2020). A continental-scale soil evaporation dataset derived from soil moisture active passive satellite drying rates. *Scientific Data*, *7*(1), 406. https://doi.org/10.1038/s41597-020-00748-z

Akaike, H. (1974). A new look at the statistical model identification. *IEEE Transactions on Automatic Control*, *19*(6), 716–723. https://doi.org/10.1109/tac.1974.1100705

Akbar, R., Short Gianotti, D. J., McColl, K. A., Haghighi, E., Salvucci, G. D., & Entekhabi, D. (2018). Estimation of landscape soil water losses from satellite observations of soil moisture. *Journal of Hydrometeorology*, *19*(5), 871–889. https://doi.org/10.1175/JHM-D-17-0200.1

Allred, B. W., Bestelmeyer, B. T., Boyd, C. S., Brown, C., Davies, K. W., Duniway, M. C., et al. (2021). Improving Landsat predictions of rangeland fractional cover with multitask learning and uncertainty. *Methods in Ecology and Evolution*, *12*(5), 841–849. https://doi.org/10.1111/2041-210x.13564

Araki, R., Morgan, B., McMillan, H., & Caylor, K. (2025). *RY4GIT/smap-drydown: v1.0: Araki et al., (2025) release*. Zenodo. https://doi.org/10.5281/ZENODO.14532741

Bassiouni, M. (2020). Global dataset of ecohydrological parameters inferred from satellite observations. Title of the publication associated with this dataset.

Bassiouni, M., Good, S. P., Still, C. J., & Higgins, C. W. (2020a). Plant water uptake thresholds inferred from satellite soil moisture. *Geophysical Research Letters*, *47*(7). https://doi.org/10.5281/zenodo.3605620

Bassiouni, M., Good, S. P., Still, C. J., & Higgins, C. W. (2020b). Plant water uptake thresholds inferred from satellite soil moisture. *Geophysical Research Letters*, *47*(7), e2020GL087077. https://doi.org/10.1029/2020gl087077

Bassiouni, M., Manzoni, S., & Vico, G. (2023). Optimal plant water use strategies explain soil moisture variability. *Advances in Water Resources*, *173*(104405), 104405. https://doi.org/10.1016/j.advwatres.2023.104405

Berg, A., & Sheffield, J. (2018). Climate change and drought: The soil moisture perspective. *Current Climate Change Reports*, *4*(2), 180–191. https://doi.org/10.1007/s40641-018-0095-0

Colliander, A., Jackson, T. J., Bindlish, R., Chan, S., Das, N., Kim, S. B., et al. (2017). Validation of SMAP surface soil moisture products with core validation sites. *Remote Sensing of Environment*, *191*(September), 215–231. https://doi.org/10.1016/j.rse.2017.01.021

Colliander, A., Reichle, R. H., Crow, W. T., Cosh, M. H., Chen, F., Chan, S., et al. (2022). Validation of soil moisture data products from the NASA SMAP mission. *IEEE Journal of Selected Topics in Applied Earth Observations and Remote Sensing*, *15*, 364–392. https://doi.org/10.1109/jstars.2021.3124743

Dong, J., Lei, F., & Crow, W. T. (2022). Land transpiration-evaporation partitioning errors responsible for modeled summertime warm bias in the central United States. *Nature Communications*, *13*(1), 336. https://doi.org/10.1038/s41467-021-27938-6

Entekhabi, D., & Rodriguez-Iturbe, I. (1994). Analytical framework for the characterization of the space-time variability of soil moisture. *Advances in Water Resources*, *17*(1), 35–45. https://doi.org/10.1016/0309-1708(94)90022-1

Fan, Y., Li, H., & Miguez-Macho, G. (2013). Global patterns of groundwater table depth. *Science*, *339*(6122), 940–943. https://doi.org/10.1126/science.1229881

Fan, Y., Miguez-Macho, G., Jobbágy, E. G., Jackson, R. B., & Otero-Casal, C. (2017). Hydrologic regulation of plant rooting depth. *Proceedings of the National Academy of Sciences of the United States of America*, *114*(40), 10572–10577. https://doi.org/10.1073/pnas.1712381114

Feldman, A. F., Konings, A., Gentine, P., Cattry, M., Wang, L., Smith, W. K., et al. (2024). Large global-scale vegetation sensitivity to daily rainfall variability. *Nature*, *636*(8042), 380–384. https://doi.org/10.1038/s41586-024-08232-z

Feldman, A. F., Koster, R. D., Cawse-Nicholson, K., Crow, W. T., Holmes, T. R. H., & Poulter, B. (2024). Soil moisture profiles of ecosystem water use revealed with ECOSTRESS. *Geophysical Research Letters*, *51*(8), e2024GL108326. https://doi.org/10.1029/2024gl108326

Feldman, A. F., Short Gianotti, D. J., Dong, J., Akbar, R., Crow, W. T., McColl, K. A., et al. (2023). Remotely sensed soil moisture can capture dynamics relevant to plant water uptake. *Water Resources Research*, *59*(2), e2022WR033814. https://doi.org/10.1029/2022wr033814

Feldman, A. F., Short Gianotti, D. J., Konings, A. G., McColl, K. A., Akbar, R., Salvucci, G. D., & Entekhabi, D. (2018). Moisture pulse-reserve in the soil-plant continuum observed across biomes. *Nature Plants*, *4*(12), 1026–1033. https://doi.org/10.1038/s41477-018-0304-9

Feldman, A. F., Short Gianotti, D. J., Trigo, I. F., Salvucci, G. D., & Entekhabi, D. (2019). Satellite-based assessment of land surface energy partitioning–soil moisture relationships and effects of confounding variables. *Water Resources Research*, *55*(12), 10657–10677. https://doi.org/10.1029/2019WR025874

Fu, Z., Ciais, P., Feldman, A. F., Gentine, P., Makowski, D., Prentice, I. C., et al. (2022). Critical soil moisture thresholds of plant water stress in terrestrial ecosystems. *Science Advances*, *8*(44), eabq7827. https://doi.org/10.1126/sciadv.abq7827

Fu, Z., Ciais, P., Wigneron, J.-P., Gentine, P., Feldman, A. F., Makowski, D., et al. (2024). Global critical soil moisture thresholds of plant water stress. *Nature Communications*, *15*(1), 4826. https://doi.org/10.1038/s41467-024-49244-7

Good, S. P., Noone, D., & Bowen, G. (2015). WATER RESOURCES. Hydrologic connectivity constrains partitioning of global terrestrial water fluxes. *Science*, *349*(6244), 175–177. https://doi.org/10.1126/science.aaa5931

Green, J. K., Seneviratne, S. I., Berg, A. M., Findell, K. L., Hagemann, S., Lawrence, D. M., & Gentine, P. (2019). Large influence of soil moisture on long-term terrestrial carbon uptake. *Nature*, *565*(7740), 476–479. https://doi.org/10.1038/s41586-018-0848-x

Greve, P., Roderick, M. L., Ukkola, A. M., & Wada, Y. (2019). The aridity index under global warming. *Environmental Research Letters*, *14*(12), 124006. https://doi.org/10.1088/1748-9326/ab5046

Hochberg, U., Rockwell, F. E., Holbrook, N. M., & Cochard, H. (2018). Iso/Anisohydry: A plant–environment interaction rather than a simple hydraulic trait. *Trends in Plant Science*, *23*(2), 112–120. https://doi.org/10.1016/j.tplants.2017.11.002

Jackson, R. B., Canadell, J., Ehleringer, J. R., Mooney, H. A., Sala, O. E., & Schulze, E. D. (1996). A global analysis of root distributions for terrestrial biomes. *Oecologia*, *108*(3), 389–411. https://doi.org/10.1007/BF00333714

Jasechko, S., Sharp, Z. D., Gibson, J. J., Birks, S. J., Yi, Y., & Fawcett, P. J. (2013). Terrestrial water fluxes dominated by transpiration. *Nature*, *496*(7445), 347–350. https://doi.org/10.1038/nature11983

Jung, M., Reichstein, M., Ciais, P., Seneviratne, S. I., Sheffield, J., Goulden, M. L., et al. (2010). Recent decline in the global land evapotranspiration trend due to limited moisture supply. *Nature*, *467*(7318), 951–954. https://doi.org/10.1038/nature09396

Konings, A. G., & Gentine, P. (2017). Global variations in ecosystem-scale isohydricity. *Global Change Biology*, *23*(2), 891–905. https://doi.org/10.1111/gcb.13389

Koster, R. D., & Suarez, M. J. (2001). Soil moisture memory in climate models. *Journal of Hydrometeorology*, *2*(6), 558–570. https://doi.org/10.1175/1525-7541(2001)002⟨0558:SMMICM⟩2.0.CO;2

Krell, N. T., Morgan, B. E., Gower, D., & Caylor, K. K. (2021). Consequences of dryland maize planting decisions under increased seasonal rainfall variability. *Water Resources Research*, *57*(9). https://doi.org/10.1029/2020wr029362

Laio, F., Porporato, A., Ridolfi, L., & Rodriguez-Iturbe, I. (2001). Plants in water-controlled ecosystems: Active role in hydrologic processes and response to water stress: II. Probabilistic soil moisture dynamics. *Advances in Water Resources*, *24*(7), 707–723. https://doi.org/10.1016/s0309-1708(01)00005-7

Laio, F., Porporato, A., Ridolfi, L., & Rodriguez-Iturbe, I. (2002). On the seasonal dynamics of mean soil moisture. *Journal of Geophysical Research*, *107*(D15), ACL8-1–ACL8-9. https://doi.org/10.1029/2001jd001252

Lei, F., Crow, W. T., Holmes, T. R. H., Hain, C., & Anderson, M. C. (2018). Global investigation of soil moisture and latent heat flux coupling strength. *Water Resources Research*, *54*(10), 8196–8215. https://doi.org/10.1029/2018wr023469

Li, W., Migliavacca, M., Forkel, M., Walther, S., Reichstein, M., & Orth, R. (2021). Revisiting global vegetation controls using multi-layer soil moisture. *Geophysical Research Letters*, *48*(11), e2021GL092856. https://doi.org/10.1029/2021gl092856

Li, Y., Guan, K., Gentine, P., Konings, A. G., Meinzer, F. C., Kimball, J. S., et al. (2017). Estimating global ecosystem isohydry/anisohydry using active and passive microwave satellite data. *Journal of Geophysical Research: Biogeosciences*, *122*(12), 3306–3321. https://doi.org/10.1002/2017jg003958

McColl, K. A., He, Q., Lu, H., & Entekhabi, D. (2019). Short-term and long-term surface soil moisture memory time scales are spatially anti-correlated at global scales. *Journal of Hydrometeorology*, *20*(6), 1165–1182. https://doi.org/10.1175/jhm-d-18-0141.1

McColl, K. A., Wang, W., Peng, B., Akbar, R., Short Gianotti, D. J., Lu, H., et al. (2017). Global characterization of surface soil moisture drydowns. *Geophysical Research Letters*, *44*(8), 3682–3690. https://doi.org/10.1002/2017GL072819

McDowell, N., Pockman, W. T., Allen, C. D., Breshears, D. D., Cobb, N., Kolb, T., et al. (2008). Mechanisms of plant survival and mortality during drought: Why do some plants survive while others succumb to drought? *New Phytologist*, *178*(4), 719–739. https://doi.org/10.1111/j.1469-8137.2008.02436.x

Meinzer, F. C., Woodruff, D. R., Marias, D. E., Smith, D. D., McCulloh, K. A., Howard, A. R., & Magedman, A. L. (2016). Mapping "hydroscapes" along the iso-to anisohydric continuum of stomatal regulation of plant water status. *Ecology Letters*, *19*(11), 1343–1352. https://doi.org/10.1111/ele.12670

O'Neill, P. E., Bindlish, R., Chan, S., Chaubell, J., Colliander, A., Njoku, E., & Jackson, T. (2021). Soil moisture active passive (SMAP) algorithm theoretical basis document level 2 & 3 soil moisture (passive) data products. Retrieved from https://nsidc.org/sites/default/files/l2_sm_p_atbd_rev_g_final_oct2021_0.pdf

O'Neill, P. E., Chan, S., Njoku, E. G., Jackson, T., Bindlish, R., & Chaubell, M. J. (2021). *SMAP L3 radiometer global daily 36 km EASE-grid soil moisture, version 8*. NASA National Snow and Ice Data Center Distributed Active Archive Center. https://doi.org/10.5067/OMHVSRGFX38O

Peng, J., Mohommed, P., Chaubell, J., Chan, s., Kim, S., Das, N., et al. (2019). *Soil moisture active passive (SMAP) L1-L3 ancillary static data, version 1*. NASA National Snow and Ice Data Center Distributed Active Archive Center. https://doi.org/10.5067/HB8BPJ13TDQJ

Porporato, A., Laio, F., Ridolfi, L., Caylor, K. K., & Rodriguez-Iturbe, I. (2003). Soil moisture and plant stress dynamics along the kalahari precipitation gradient. *Journal of Geophysical Research*, *108*(D3), 4127. https://doi.org/10.1029/2002jd002448

Rahmati, M., Amelung, W., Brogi, C., Dari, J., Flammini, A., Bogena, H., et al. (2024). Soil moisture memory: State-Of-The-Art and the way forward. *Reviews of Geophysics*, *62*(2), e2023RG000828. https://doi.org/10.1029/2023RG000828

Reichle, R., De Lannoy, G., Koster, R., Crow, W., Kimball, J., Liu, Q., & Bechtold, M. (2022). *SMAP L4 global 3-hourly 9 km EASE-grid surface and root zone soil moisture geophysical data, version 7*. NASA National Snow and Ice Data Center Distributed Active Archive Center. https://doi.org/10.5067/EVKPQZ4AFC4D

Rodriguez-Iturbe, I., Porporato, A., Ridolfi, L., Isham, V., & Coxi, D. R. (1999). Probabilistic modelling of water balance at a point: The role of climate, soil and vegetation. *Proceedings of the Royal Society of London. Series A: Mathematical, Physical and Engineering Sciences*, *455*(1990), 3789–3805. https://doi.org/10.1098/rspa.1999.0477

Rondinelli, W. J., Hornbuckle, B. K., Patton, J. C., Cosh, M. H., Walker, V. A., Carr, B. D., & Logsdon, S. D. (2015). Different rates of soil drying after rainfall are observed by the SMOS satellite and the south fork in situ soil moisture network. *Journal of Hydrometeorology*, *16*(2), 889–903. https://doi.org/10.1175/jhm-d-14-0137.1

Sehgal, V., Gaur, N., & Mohanty, B. P. (2021). Global surface soil moisture drydown patterns. *Water Resources Research*, *57*(1). https://doi.org/10.1029/2020wr027588

Shellito, P. J., Small, E. E., Colliander, A., Bindlish, R., Cosh, M. H., Berg, A. A., et al. (2016). SMAP soil moisture drying more rapid than observed in situ following rainfall events. *Geophysical Research Letters*, *43*(15), 8068–8075. https://doi.org/10.1002/2016GL069946

Shellito, P. J., Small, E. E., & Livneh, B. (2018). Controls on surface soil drying rates observed by SMAP and simulated by the NOAH land surface model. *Hydrology and Earth System Sciences*, *22*(3), 1649–1663. https://doi.org/10.5194/hess-22-1649-2018

Singer, M., Asfaw, D., Rosolem, R., Cuthbert, M. O., Miralles, D. G., Miguitama, E. Q., et al. (2020). *Hourly potential evapotranspiration (hPET) at 0.1degs grid resolution for the global land surface from 1981-present*. University of Bristol. https://doi.org/10.5523/BRIS.QB8UJAZZDA0S2AYKKV0OQ0CTP

Singer, M. B., Asfaw, D. T., Rosolem, R., Cuthbert, M. O., Miralles, D. G., MacLeod, D., et al. (2021). Hourly potential evapotranspiration at 0.1° resolution for the global land surface from 1981-present. *Scientific Data*, *8*(1), 224. https://doi.org/10.1038/s41597-021-01003-9

Small, E. E., Badger, A. M., Abolafia-Rosenzweig, R., & Livneh, B. (2018). Estimating soil evaporation using drying rates determined from Satellite-Based soil moisture records. *Remote Sensing*, *10*(12), 1945. https://doi.org/10.3390/rs10121945

Stocker, B. D., Zscheischler, J., Keenan, T. F., Prentice, I. C., Seneviratne, S. I., & Peñuelas, J. (2019). Drought impacts on terrestrial primary production underestimated by satellite monitoring. *Nature Geoscience*, *12*(4), 264–270. https://doi.org/10.1038/s41561-019-0318-6

Tardieu, F., & Davies, W. J. (1993). Integration of hydraulic and chemical signalling in the control of stomatal conductance and water status of droughted plants. *Plant, Cell and Environment*, *16*(4), 341–349. https://doi.org/10.1111/j.1365-3040.1993.tb00880.x

Tardieu, F., & Simonneau, T. (1998). Variability among species of stomatal control under fluctuating soil water status and evaporative demand: Modelling isohydric and anisohydric behaviours. *Journal of Experimental Botany*, *49*(Special_Issue), 419–432. https://doi.org/10.1093/jxb/49.Special_Issue.419

Teuling, A. J., & Troch, P. A. (2005). Improved understanding of soil moisture variability dynamics. *Geophysical Research Letters*, *32*(5), L05404. https://doi.org/10.1029/2004GL021935

Teuling, A. J., Uijlenhoet, R., Hupet, F., & Troch, P. (2006). Impact of plant water uptake strategy on soil moisture and evapotranspiration dynamics during drydown. *Geophysical Research Letters*, *33*(3). https://doi.org/10.1029/2005GL025019

Tso, C.-H. M., Blyth, E., Tanguy, M., Levy, P. E., Robinson, E. L., Bell, V., et al. (2023). Multiproduct characterization of surface soil moisture drydowns in the United Kingdom. *Journal of Hydrometeorology*, *24*(12), 2299–2319. https://doi.org/10.1175/JHM-D-23-0018.1

Virtanen, P., Gommers, R., Oliphant, T. E., Haberland, M., Reddy, T., Cournapeau, D., et al. (2020). SciPy 1.0: Fundamental algorithms for scientific computing in python. *Nature Methods*, *17*(3), 261–272. https://doi.org/10.1038/s41592-019-0686-2

Wilkening, J. V., Feng, X., Dawson, T. E., & Thompson, S. E. (2024). Different roads, same destination: The shared future of plant ecophysiology and ecohydrology. *Plant, Cell and Environment*, *47*(9), 3447–3465. https://doi.org/10.1111/pce.14937